

Cosmic-Ray Acceleration in Supernova Remnants

Vera G. Sinitsyna * and Vera Y. Sinitsyna

P.N. Lebedev Physical Institute, Russian Academy of Science, Moscow 119991, Russia

* Correspondence: sinits@sci.lebedev.ru

Abstract: Supernova Remnants (SNRs) are generally believed to produce the cosmic rays in our Galaxy due to the powerful supernova blast waves generated by expanding SNRs. In contrast to the leptonic cosmic-ray component that is clearly seen by the SNR emission in a wide wavelength range, from radio to high-energy γ -ray, the hadronic cosmic-ray component can be detected only by very high energy γ -ray emission. Galactic SNRs of various ages have been intensively studied at very high energies. Among them are the shell-type SNRs: Tycho's SNR, Cas A, IC 443, γ Cygni SNR, G166.0+4.3. The results of investigations of listed SNRs obtained in observations at 800 GeV–100 TeV energies by SHALON telescope are presented with spectral energy distribution and emission maps compared with experimental data from the wide energy range, from radio to high-energy gamma-rays. The TeV emission maps of supernova remnants obtained by SHALON are overlaid with ones viewed in radio-frequencies and X-rays to reveal SNR's essential features which can lead to the effective generation of cosmic rays. The presented experimental data from high and very high energies are considered together with theoretical predictions to test the cosmic ray origin in these objects.

Keywords: supernova remnants; cosmic rays; Cas A; Tycho's SNR; γ Cygni SNR; IC 443; G166.0+4.3; multi-wavelength electromagnetic emission

1. Introduction

The investigation of supernova remnants (SNRs) across the electromagnetic spectrum from radio up to very high energy gamma-rays touches on one of the unresolved problems of modern astrophysics, namely the origin of cosmic rays and the Galaxy's contribution to the overall cosmic ray spectrum. Supernova Remnants (SNRs) are widely considered to be unique candidates for cosmic-ray sources in our Galaxy [1–3], as supernova explosion can provide the kinetic energy enough to generate relativistic cosmic rays. According to the theory of diffusive shock acceleration [2,4–6] it is suggested that particles can be generated by the shocks of SNRs up to energies of PeV. The charged cosmic ray particles have lost all directional information about the place of origin before reaching the Earth due to the galactic magnetic fields. So, the searches for the sites of the generation of cosmic rays are possible with gamma-rays as they are the neutral secondary products of cosmic ray acceleration. The presence of the electron cosmic-ray component is clearly seen by the emission generated by it in an SNR in a wide energy range, from radio to high-energy gamma-rays, while the nuclear cosmic-ray component can be detected only by very high-energy gamma-ray emission.

Galactic SNRs of various ages and of different progenitor systems have been intensively studied at very high energies. The results of long-term observations of different SNRs at very high energies using the SHALON mirror Cherenkov telescope are presented. The SHALON telescope systems are high-altitude imaging Cherenkov telescopes for the 800 GeV–100 TeV gamma-ray astronomy [7–10]. SHALON telescopes are located in the Tien-Shan mountains at an altitude of 3340 m above sea level. This site has an optical quality of atmosphere optimal for observing Cherenkov light of extensive air showers. The optical reflector of a SHALON telescope is a tessellated structure consisting of 38 identical spherical mirrors characterized with >96% reflectivity, composing a total reflecting area of



Citation: Sinitsyna, V.G.; Sinitsyna, V.Y. Cosmic-Ray Acceleration in Supernova Remnants. *Universe* **2023**, *9*, 98. <https://doi.org/10.3390/universe9020098>

Academic Editor: Daniele Fargion

Received: 14 December 2022

Revised: 4 February 2023

Accepted: 8 February 2023

Published: 15 February 2023



Copyright: © 2023 by the authors. Licensee MDPI, Basel, Switzerland. This article is an open access article distributed under the terms and conditions of the Creative Commons Attribution (CC BY) license (<https://creativecommons.org/licenses/by/4.0/>).

11.2 m². The accuracy of the mirror surface is 5λ , which is defined by a point spot dispersion ($\lambda = 500$ nm) and dispersion of focal length of $\leq 1\%$ [11]. An imaging camera placed at the focus of the reflector consists of 144FEU-85 photomultiplier tubes in a close-packed square arrangement and has a large field of view of $>8^\circ$. This type of PMTs demonstrated the sustainability and stability of characteristics in temperatures ranging from -20° to $+40^\circ$. The Cherenkov telescope performance, observation methods of data taking, data analysis, etc., is summarized by its angular resolution and sensitivity to the gamma-ray flux. The accuracy of the determination of the coordinates of the source of the individual gamma-ray shower in SHALON experiment is $\sim 0.07^\circ$ [9], and it is increased by a factor of ~ 10 after the additional joint shower processing [9] using deconvolution algorithm [12]. The telescope's sensitivity is defined as the minimum flux of gamma-rays for a statistically significant detection. Here, the minimum flux of gamma-rays for the 50 h of observation of a point-like source in SHALON experiment at a confidence level of 5σ calculated according to formula 17 from the paper [13] is estimated. Thus, the telescope sensitivity to detect a point-like source at an of 5σ for 50 h of observation is determined with an integral flux of $2.1 \times 10^{-13} \text{ cm}^{-2} \text{ s}^{-1}$ at the energy of 1 TeV (for details see [9,10,14,15]).

Here, the results of observations of Tycho's SNR, Cas A, IC 443, γ Cygni SNR, G166.0+4.3 at 800 GeV–100 TeV with SHALON telescope are presented together with data from the MeV–GeV investigation by Fermi LAT, both compared with estimations and models of high energy emission generation. The SNRs' TeV emission maps obtained by SHALON are overlaid with ones obtained with X-ray experiments Chandra ACIS, ROSAT, XMM-Newton, and radio-observations from Canadian Galactic Plane Survey DRAO in order to compare SNR TeV γ -ray morphology with structures viewed through the X-ray and radio images and revealed its essential features which can lead to the effective generation of cosmic rays. These results are analyzed to examine the scenarios of leptonic and hadronic production of gamma-ray emission in supernova remnants. The overall experimental data collected at the high and very high energy ranges can help to resolve the evolution of the individual SNRs' features and spectral energy distributions in various kinds of ambient environments and reveal the characteristic signature of cosmic ray origin.

2. Cas A

The Type IIb supernova explosion which occurred approximately 1680 gave a rise to Cas A supernova remnant. It is supposed that the progenitor of Cas A is a red supergiant that hydrogen envelope was mostly lost through strong stellar winds before the supernova occurred [16]. The analysis of the proper motion of optical filaments gave distance estimations of 3.4 kpc. It has an angular size of 5 arcmin. This youngest Galactic SNR is considered to be the best target to test a hypothesis of CR origin in supernova remnants because of the overall detailed studies. Cas A has been intensively studied through multi-wavelength observations in radio, X-rays, and MeV–TeV energy ranges which aimed to reveal the explosion footprints and interactions with the surrounding medium.

The location of the reverse shock is visible due to its interaction with SNR ejecta that is observed in radio emission of 1.7 arcmin size [17,18]. Also, the faint radio emission of 2.5 arcmins [19] originated from the synchrotron radiation of electrons moving in a magnetic field. The nonthermal X-ray emission was detected at the energy of 4–6 keV by Chandra [20] and then through the 15–20 keV by NuSTAR [21] up to 220 keV energy visible by INTEGRAL [22]. The observed X-ray emission mostly follows the large-scale SNR features detected at radio frequencies and can be explained by the expanded shocks within the interpretation of synchrotron radiation produced by electrons shock-accelerated to an energy up to 40–60 TeV.

High energy gamma-ray emission from Cas A was detected by Fermi-LAT in the MeV–GeV energy range [23]. The differential photo spectrum measured in the 12-year observations between the 100 MeV and 1000 GeV is described by a power law with an index of -1.97 ± 0.0153 [24]. Also, Cas A was detected at the energies of several TeV (see e.g., [25]). The high energy gamma-rays can be produced by energetic electrons, via

inverse-Compton (IC) scattering for example. So, to determine whether the mechanism of proton acceleration at the shock is efficient or not, the gamma-ray emission spectrum should be measured up to energies more than 10 TeV [26].

Cas A was observed with SHALON from 2010–2014 yy [27,28] and the data-set of the 76.7 h was included in the analysis. The observations were taken during moonless nights with zenith angles from 13° to 35° using the standard procedure of SHALON experiment with the simultaneous source and background tracking mode [9,10,27]. The observations of the Cas A SNR by SHALON revealed the γ -ray emission from this object at the level of 19.4σ [15,27,28] with an integral flux of $I_{CasA}(> 0.8 \text{ TeV}) = (0.64 \pm 0.10) \times 10^{-12} \text{ cm}^{-2} \text{ s}^{-1}$ using the standard procedure of SHALON experiment (e.g., [10]). The description of differential gamma-ray energy spectrum between the 800 GeV and 30 TeV with hard power law with an exponential cutoff is preferred as: $dF/dE = N_0 \times (E/\text{TeV})^k \times \exp(-E/E_{cutoff})$, where $N_0 = (9.61 \pm 0.10) \times 10^{-13} \text{ TeV}^{-1} \text{ cm}^{-2} \text{ s}^{-1}$, $k = -1.97 \pm 0.21$ and $E_{cutoff} = 9.5 \pm 3.5 \text{ TeV}$ ($\chi^2 = 1.09$ at DoF = 6). A power-law fit to the data points in the form of $dF/dE = (1.1 \pm 0.10) \times 10^{-12} \times (E/\text{TeV})^{-2.53 \pm 0.12}$ gives a χ^2 of 0.82 for 7 degrees of freedom.

The characteristics of gamma-ray emission in the energy range of 0.8–30 TeV from Cas A are presented in Figure 1, top with spectral energy distribution by SHALON (\blacktriangle) in comparison with theoretical predictions [23,26,29] and available experimental data [24,30–33]. Solid lines at Figure 1 show the very high energy γ -ray spectra of hadronic origin [23,26,31], whereas the dashed line is a leptonic production of gamma-rays [23]. The solid line shows the spectrum of gamma-ray emission from Cas A produced in the assumption of proton acceleration spectrum with $k_p = -2.17$ and the case of softer proton spectrum with index $k_p = -2.3$ is presented by the solid grey line. The dashed line presents the spectrum within the leptonic model of gamma-ray production via the IC scattering with $B = 0.12 \text{ mG}$ which can explain the observed GeV flux and predicts the TeV spectrum with cut-off energy about 10 TeV. The hard spectrum below 1 TeV viewed by Fermi LAT and the detection of γ -ray emission at 5–30 TeV by SHALON would favor the π^0 -decay origin of the γ -rays in Cas A. Also, the hadronic origin of the MeV-TeV detected gamma-ray emission was confirmed in the one-zone hadron-dominated scenario [31]. The considered scenario with the hadronic model supposes the 2–5% efficiency of cosmic ray acceleration [31].

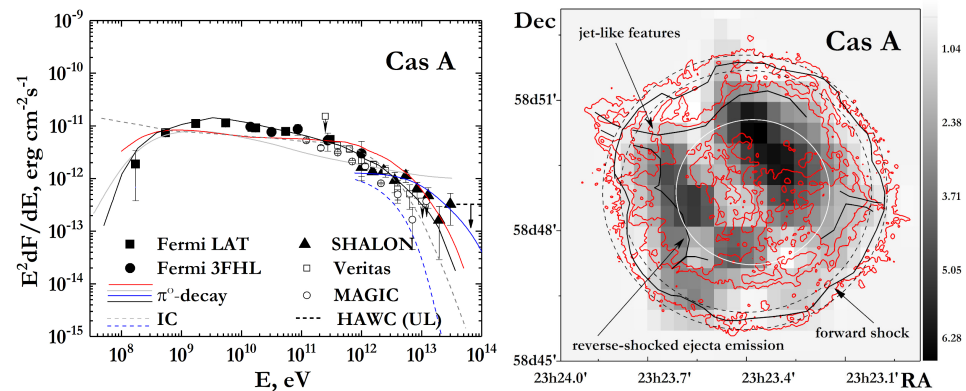


Figure 1. (left): Spectral energy distribution of Cas A SNR: \blacktriangle at TeV energies show the data from SHALON observations. (right): Emission maps of SNR by SHALON (grey scale). Red lines show the X-ray emission by Chandra (see text for the description).

The Cas A structure in the energy range of 0.8–30 TeV viewed by SHALON (grey scale) is presented in Figure 1, right. It is overlaid with an X-ray image of Cas A by Chandra (red lines). Two remarkable features of Cas A nonthermal X-ray emission are found [20]. First, throughout the remnant, there is an existing 4–6 keV emission of mostly circular structure that is probably synchrotron radiation generated at the forward shock. Another one is the emission of 1.78–2.0 keV from the reverse-shocked ejecta region with viewed in 6.52–6.95 keV jet-like features located in the northeast and in the southwest. The position

of this noncircular component is shown with a black contour. The reverse and forward shock regions, as well as the jet-like features [20], are marked with arrows.

The Cas A structure obtained with the multiwavelength observations has clear signs of young SNRs, which are expected to be a shell formed with the explosion blast wave moving into the circumstellar medium with magnetic fields, as well as another one due to the decelerating and compressing the outflowing ejecta. In observations in radio and X-rays, both features were detected. The forward and reverse shocks in Cas A were identified by [34]. In Figure 1 (right), these features are marked with black lines and a white circle. It was shown that the nonthermal radio emission at 4.4 GHz from the VLA mostly comes from the bright radio ring with an angular radius of $\sim 1.8'$ which is believed to be related to the reverse shock propagating into the supernova ejecta. Then, this radio emission forms the faint outer plateau of a $2.5'$ angular radius. Also, it was found that the X-ray line emissivity radial profile roughly coincides with the bright radio ring. A high-energy X-ray continuum emission map of Cas A at 4–6 keV by Chandra reveals the faint filamentary structures at $2.5'$, close to the boundary of the radio plateau. These X-ray structures correspond to the position of the forward shock which propagates in the circumstellar medium (see black lines and black dashed-line circles in Figure 1, right). The TeV gamma-ray emission region lays within the position of reverse shock (inner white circle) reported by [34] and also corresponds to the observed bright radio ring.

The observed impact structure of the SNR shell confirms the idea of cosmic ray production in our Galaxy through the mechanism of diffusion impact acceleration [4,6], which predicts that the particle spectrum is consistent with the observed cosmic ray spectrum, including the corrections on propagation effects.

The nonthermal radiation of the described structures viewed in radio is direct evidence of the existence of a large number of relativistic shock-accelerated electrons up to energies of ~ 10 TeV. The hard X-ray emission from position $2.5'$ is interpreted as synchrotron radiation of electrons accelerated at the forward shock to energies of ~ 40 – 60 TeV. The properties of detected emission also imply that the magnetic fields in the observable shocks are extremely amplified compared with that of ejecta expanding through the circumstellar medium. These effective magnetic fields highly influence the acceleration of cosmic rays and their dynamics in SNR.

As mentioned above, the efficiency of the acceleration of hadronic cosmic-ray can be determined with TeV gamma-ray emission. If protons are efficiently accelerated in Cas A, then the π^0 -decay gamma-ray spectrum because of inelastic collisions with the background nuclei must extend beyond 1 TeV with a hard power-law spectrum. The analysis of Cas A dynamics together with the detected thermal X-ray emission showed that the blast wave had already passed the swept-up red supergiant wind shell from the progenitor and are presently propagating through the slow red supergiant wind. This results in the circumstellar material mass swept up by the SNR shock being enough to provide a gamma-ray flux from the π^0 -decay at a level enough for the detection. Detailed studies of spectral and morphological features of Cas A in the wide energy range within the diffusive shock acceleration mechanism were performed in [26,29].

The nonlinear kinetic model for diffusive shock acceleration in Cas A [26] was applied to describe the spectral and structural features of this SNR viewed in nonthermal emission, including ones at high energies. In this model, the Cas A properties observed at radio, X-rays as well as high-energy gamma-rays are described within the assumption of the blast wave of the supernova explosion as a main source of the high-energy particles. In case of effective acceleration, the mechanism provides the cosmic rays up to above 10^{17} eV.

In particular, to produce the shock-accelerated electrons generating a very steep radio spectrum and distributed within the swept-up shell corresponding to the bright radio ring as observed with VLA (see [34] for details) the shock must be strongly modified by accelerated protons which are efficiently injected into the acceleration process. On the other hand, due to the high magnetic field arising due to the amplification by cosmic rays near shock, significant synchrotron losses of relativistic electrons lead to well reproducing

spectral shape at radio to X-ray energies. The experimental evidence of the effectively of acceleration of the cosmic rays with SNR has been well demonstrated with Cas A characteristics viewed in very high energies. The calculation of the spectrum of very high energy gamma rays from Cas A generated by the hadronic cosmic rays' collisions with the gas nuclei shows that it extends up to 30 TeV and has a hard shape (see blue line in Figure 1 left). In contrast, gamma-ray fluxes of the leptonic origin have a cutoff at about 1 TeV (see dashed blue line in Figure 1 left). Thus, the characteristics of the spectral energy distribution of gamma-rays at 800 GeV–40 TeV (Figure 1 left) detected from the regions seen in Figure 1, right are the evidence of acceleration of the hadronic cosmic rays in shells of supernova remnants up to 10^{17} eV.

In the [29] the nonlinear diffusive shock acceleration model was applied to Cas A to reproduce spectral and morphological features of radio, X-ray, and gamma-ray emission generated by electrons, protons, and specific ions accelerated by both the forward and reverse shocks of this SNR. The forward and reverse shocks are considered to be propagating through the circumstellar medium and supernova ejecta, respectively those parameters are specific for the case of Cas A and inferred from the observations in radio and X-ray energy ranges. The shape of the observed broadband energy spectra of gamma-rays implies strong amplification of the magnetic field at the forward and reverse shocks which are implemented in the model.

The gamma-emission spectral shape calculated in the hadronic model is in good agreement with the measurements of the spectrum at high and very high energies (see red line in Figure 1 left). Whereas the very-high-energy gamma-ray spectrum in the leptonic scenario of gamma-ray emission production is steeper than one observed with experiments at TeV energy range including the SHALON data, and can't reproduce a sharp decline of the spectrum below 1 GeV, observed by Fermi LAT.

The radio, X-ray, and gamma-ray components of the emission peak at a $1.7'–2.0'$ radius correspond to the position of reverse shock. The radial profile of 1 TeV gamma-rays calculated within this hadronic model shows that most of the very-high-energy emission from the π^0 -decay comes from the regions of $1.5'–2'$, which agrees with one observed at >800 GeV by SHALON (see Figure 1, right).

Results of these calculations demonstrate that the observational properties of Cas A are well reproduced by the hadronic model with significant contribution of both the forward and reverse shocks in the generation of broadband emission. This model considers a very high efficiency of particle acceleration in Cas A, the value of which is up to 25% of the supernova explosion energy. However, the energy of accelerated particles cannot exceed $10^{14}–10^{15}$ eV.

3. Tycho's SNR

Tycho's supernova remnant is of a rare Galactic SNR subclass known as historical supernovae that were observed by Tycho Brahe in 1572. The available data collected since the SN appearance and further investigations at X-rays suggested a standard Type Ia origin by the thermonuclear explosion of a white dwarf star in a close binary [35] without any neutron star formation. Tycho's SNR has been widely studied across the electromagnetic spectrum. However, the distance is still uncertain, and its estimations vary mostly from 2 to 4 kpc [36]. Also, the accurate characteristics of the interstellar medium around the remnant are not known either. Non-thermal emission from the Tycho SNR has been detected in radio. These studies in radio frequencies show a shell-like morphology of Tycho's SNR. The non-thermal X-ray emission from Tycho's SNR has been revealed in the Chandra experiment. Observations show the structure of SNRs' rim concentrated morphology, and it was interpreted as evidence of electron acceleration. The Tycho's shape in both the radio frequencies and in X-rays is roughly spherical, which makes it useful for modeling. The expansion rate measurements in radio and X-ray suggest that Tycho is in a pre-Sedov evolutionary state and show the conditions for particle acceleration.

Also, Tycho’s SNR X-ray images measured by Chandra [37] demonstrate that the supersonic expansion of the stellar debris has created two shock waves: the blast wave that moves outward into the interstellar gas, and the reverse shock that moves back into the debris. This type of shock and the contact discontinuity surface displacement makes the cosmic ray acceleration at the supernova shock very efficient. In the 12-year Fermi-LAT measurements, the gamma-ray emission from Tycho’s SNR has been detected in the energy range of 100 MeV–300 GeV its spectrum is described by a power law with an index of -2.22 ± 0.06 .

Tycho’s SNR was detected at energies of >800 GeV in observations of the 1996 year by SHALON [38,39] with 17.9σ determined by [13]. The Tycho’s SNR integral flux above 0.8 TeV is $(0.52 \pm 0.04) \times 10^{-12} \text{ cm}^{-2} \text{ s}^{-1}$. The data was taken with SHALON between 1996 to 2010 year [15,27,38] during moonless nights with zenith angles from 16° to 35° and the 126.5 h of observations were included in the analysis.

The differential spectrum at energies of >0.8 TeV can be described by a power-law distribution $dF/dE = (3.2 \pm 0.36) \times 10^{-13} (E/\text{TeV})^{-1.95 \pm 0.68}$. This fit gives a χ^2 of 2.2 for ten degrees. So, the energy spectrum of gamma-rays in the energy range from 800 GeV to 80 TeV is well described by the power law with exponential cutoff $dF/dE = (2.21 \pm 0.11) \times 10^{-13} (E/1.1\text{TeV})^{-1.62 \pm 0.19} \times \exp(-E/(35 \pm 5) \text{ TeV}) \text{ TeV}^{-1} \text{ cm}^{-2} \text{ s}^{-1}$ with $\chi^2/\text{DoF} = 1.10$ (with $\text{DoF} = 9$). As the TS value determined as $2\ln(\mathcal{L}(\text{CutoffPowerLaw})/\mathcal{L}(\text{PowerLaw}))$ is 11.7, the source spectrum is considered to be better described by a power law with an exponential cutoff with the parameter presented above. The differential photon spectrum was obtained with VERITAS in the energy range from 1 to 10 TeV. The shape is consistent with a power law $dN/dE = C(E/3.42\text{TeV})^\Gamma$, where $\Gamma = 1.92 \pm 0.52_{\text{stat}} \pm 0.30_{\text{sys}}$ and $C = (1.55 \pm 0.43_{\text{stat}} \pm 0.47_{\text{sys}}) \times 10^{-14} \text{ cm}^2 \text{ s}^{-1} \text{ TeV}^{-1}$ with $\chi^2 = 0.6$ for 1 degree of freedom [40]. The Tycho’s SNR gamma-ray emission characteristics were measured in the energy range of 0.8–80 TeV. Figure 2, top shows Tycho’s SNR spectral energy distribution by SHALON (\blacktriangle) in comparison with theoretical predictions [5] and other experimental data [24,30,40]. Tycho’s SNR structure in the energy range of 0.8–80 TeV obtained by SHALON is presented in greyscale in Figure 2 together with an X-ray emission map by Chandra (red lines). The inner and outer black contours in Figure 2 show the location of the reverse shock and blast wave, respectively [37]. The combination of the X-ray emission map with the TeV data by SHALON shows the localization of TeV emission regions relative to the position of forward and reverse shock (black lines) in Tycho’s SNR.

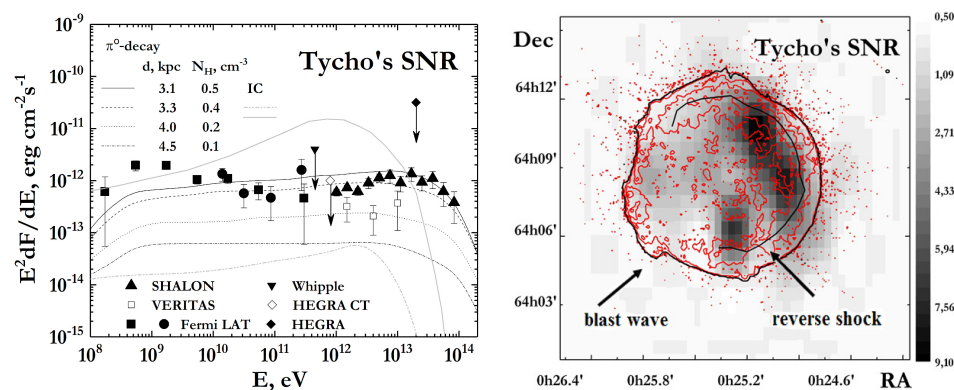


Figure 2. (left): Spectral energy distribution of Tycho’s SNR: \blacktriangle at TeV energies show the data from SHALON observations. (right): Emission map of SNR by SHALON (grey scale). Red lines show the X-ray emission by Chandra (see text for the description).

The high and very high spectral energy distribution of Tycho’s SNR is presented in the 100 MeV–80 TeV region (Figure 2, left). A nonlinear kinetic model of cosmic-ray acceleration in SNRs (see e.g., [5]) was applied to Tycho’s SNR to describe its spectral properties and find the origin of the gamma-ray emission in this object. The black lines in Figure 2 show the results of the calculation of spectral energy distribution of gamma-ray of dominantly

hadronic origin from [5] for the different source distances and ISM density N_H . The grey lines in Figure 2 show the calculations of the leptonic origin of gamma-ray emission from the Inverse Compton scattering using the varying parameters from [5].

The gamma-ray fluxes originating from the Inverse Compton scattering have a sharp cut-off above few TeV (see Figure 2), and the plateau shape below the 1 GeV. While the high energy photon spectrum from the π^0 -decay production, extends up to >30 TeV, and a sharp decline below 1 GeV. Thus, the detection of 0.8–80 TeV γ -ray emission from Tycho's SNR by SHALON [27] (Figure 2), and a sharp decline of the spectrum below 1 GeV observed by Fermi-LAT is the evidence of the hadronic origin of the high energy photons in this object. Also, to find such SNR parameters like distance and the interstellar medium density (ISM) density N_H , the model results were compared with the gamma-ray spectral energy distribution observed by SHALON at 0.8–100 TeV. As a result, the distance of 3.1–3.3 kpc and ISM density $N_H = 0.5 \text{ cm}^{-3}$ was obtained from the SHALON data within the nonlinear kinetic model. The same parameter values can be obtained from the model [41] reproducing Tycho's SNR structure visible in X-rays by Chandra (see red contours in Figure 2).

4. γ Cygni SNR

γ Cygni SNR shell-type supernova remnant located in the active Cygnus region is older than Cas A and Tycho's SNR and considered as a middle-aged SNR at ~ 5000 – 7000 years [42] which is in an early phase of adiabatic expansion. The distance is estimated as ~ 1.5 – 1.7 kpc due to the HI velocity measurements, and association with the V444 Cyg binary. γ Cygni SNR has been widely studied in radio by NRAO, Algonquin Radio Telescope, DRAO Synthesis Telescope and X-rays with ASCA, ROSAT, Chandra experiments [43–46]. A bright source of high energy gamma-rays at the position of γ Cygni SNR was detected by EGRET [47]. γ Cygni SNR has a shell-like radio and X-ray structures of $\sim 1^\circ$ diameter [42], but has a different in morphology. It was shown that the X-ray emission is dominated by shock-heated gas [48]. Also, the extended source of GeV gamma-emission matching the radio size of γ Cygni SNR was detected by Fermi-LAT [49]. The observed features of this SNR suggested that shock interactions could cause a very high energy emission in γ Cygni SNR.

During the long-term observations of Cygnus Region the SHALON field of view contains γ Cygni SNR as it located at $\sim 2^\circ$ South-West from the object Cyg X-3 which is the prime target of these investigations. Thus, due to the large telescopic field of view ($>8^\circ$) the observations of Cyg X-3 is naturally accompanied by the observations of γ Cygni SNR. As a result, 245 h of observations with zenith angles from 6° to 33° taken during the period from 1995 to 2016 year were included in the analysis. γ Cygni SNR was detected above 800 GeV in SHALON experiment [15,28,50] with an integral flux of $(1.27 \pm 0.11) \times 10^{-12} \text{ cm}^{-2} \text{ s}^{-1}$ at the level of 15.8σ determined by the method of [13].

Because of the less collection field of view for γ Cygni SNR observations compared to the standard procedure of SHALON experiment [9,10,27] the obtained signal significance for this SNR is less than one for the source with similar flux and spectrum index obtained in the same observation hours. The corrections for the effective field of view were made to calculate source flux and energy spectrum.

The power-law fit to the data points of γ Cygni SNR differential spectrum at energies of >0.8 TeV: $dF/dE = (1.13 \pm 0.16) \times 10^{-12} (E/\text{TeV})^{-2.43 \pm 0.26}$ with gives χ^2 of 11.8 for ten degrees. Thus, the energy spectrum of gamma-rays in the energy range from 800 GeV to 50 TeV is well described by the power law with exponential cutoff $dF/dE = N_0 \times E^k \exp(-E/E_{cutoff})$, where $N_0 = (0.93 \pm 0.12) \times 10^{-12} \text{ TeV}^{-1} \text{ cm}^{-2} \text{ s}^{-1}$, $k = -2.13 \pm 0.14$ and $E_{cutoff} = 22.7 \pm 4.9$ TeV. This fit results in χ^2 of 1.95 for nine degrees. As the TS value determined as $2 \ln(\mathcal{L}(\text{CutoffPowerLaw})/\mathcal{L}(\text{PowerLaw}))$ is 86.8, the source spectrum is considered to be well described by a power law with an exponential cutoff with the parameter presented above. The spectral energy distribution of γ Cygni SNR and its γ -ray emission map were measured in the energy range of 0.8–60 TeV and presented in Figure 3.

The main contribution to the TeV γ -ray fluxes is given by the regions correlated with the North-West and South-East parts of the shell which are visible by CGPS DRAO [51] at radio frequencies of 1420 MHz (red contours in Figure 3). The 10 GeV–2 TeV emission by Fermi-LAT [49] is detected from the shells of γ Cygni SNR (blue lines in Figure 3). VERITAS [52] detected the VERJ2019+407 source at 200 GeV coincides with the position of the northern part of γ Cygni SNR shell. The γ Cygni SNR region was studied in HAWC experiment in TeV energy range. 3HWC J2020+403 object of the third HAWC catalogue [53] is likely associated with VER J2019+407 and could be related with TeV emission from γ Cygni SNR [54]. The bow-tie shaped area in Figure 3 shows the spectral energy distribution of 3HWC J2020+403 by HAWC.

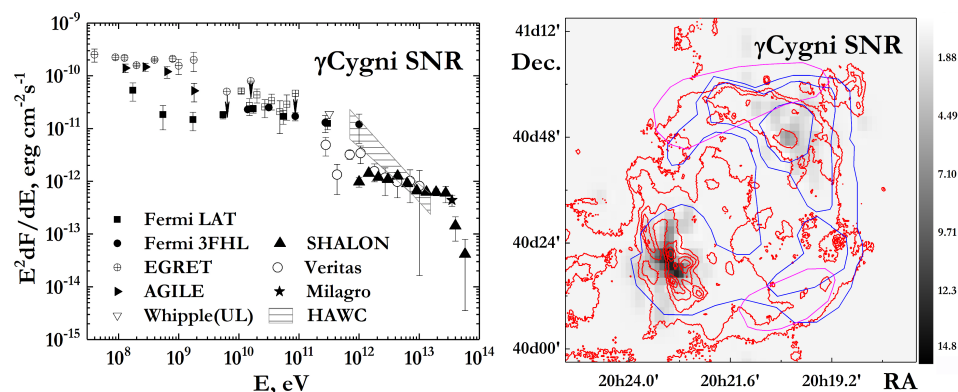


Figure 3. (left): Spectral energy distribution of γ Cygni SNR: \blacktriangle at TeV energies show the data from SHALON observations. (right): Emission map of SNRs by SHALON (grey scale). Red lines show Canadian Galactic Plane Survey DRAO data; magenta lines are the X-ray data by ROSAT, and blue lines show MeV-GeV emission regions by Fermi LAT (see text for the description).

The overall γ Cygni SNR characteristics detected in radio, X-rays as well as TeV gamma-rays can be a result of the shocks at the interaction of the supernova ejecta and the surrounding medium. First, the GeV-TeV gamma-ray emission could be generated via inverse-Compton scattering of shock-accelerated electrons which should also produce synchrotron radiation visible in the X-ray non-thermal power-law in the spectrum. However, no non-thermal component of the X-ray spectrum was detected from the location of the North-West part of the TeV shell [55] and no source of the X-ray emission was detected at the position of South-East TeV emission region (see ROSAT for X-rays in Figure 3 magenta lines).

Also, the shock acceleration of hadrons interacting with the target material can produce the TeV γ -ray emission. The estimations given in [56] show that the density of target material in the SNR surroundings is enough to produce the observable TeV gamma-ray flux via the shock acceleration of hadrons in both regions presented in Figure 3. Thus, the detection of γ -ray emission at 0.8–60 TeV from the North-West and South-East shells of γ Cygni SNR by SHALON would favor the hadronic origin of the γ -rays in this supernova remnant.

5. IC 443 SNR

IC 443 is a supernova remnant of the uncertain age that varies from 3–4 kyr up to 20–30 kyr at distance assumed as ~ 1.5 kpc. It is a core-collapse explosion SNR that demonstrates evidence of interactions with molecular clouds [57] and atomic clouds [58]. IC 443 is widely considered a candidate for the hadronic cosmic-ray source due to the close placement of the dense shocked molecular clouds and detected GeV-TeV γ -ray emission from this SNR.

IC 443 is a complex shape SNR having two roughly spherical different radius half-shells and of $\sim 45'$ extent viewable as a radio synchrotron emission. IC 443 has a rim-brightened shape at its eastern part, but the opposite side is dimmer. IC 443 has an optical range appearance similar to the radio one. In X-rays IC 443 has a peculiar morphology.

X-ray emission of IC 443 is a thermal centrally peaked within the radio rim, but with no evidence of limb-brightened shells. The unidentified source of 100 MeV to 30 GeV gamma-emission located near the center of the IC 443 shell was detected by EGRET [47]. The extended gamma-ray emission of 100 MeV–1 TeV within the radio shells was detected with the Fermi-LAT 12-year observation data [24].

IC 443 was detected at 800 GeV–10 TeV by SHALON (see [15,28,59] with an integral flux of $(1.53 \pm 0.22) \times 10^{-12} \text{ cm}^{-2} \text{ s}^{-1}$ and statistical significance of 10.9σ [13] using the standard procedure of SHALON experiment. The data were taken during 2011, 2013–2016 years in the observations with zenith angles from 20° to 35° . The 26.7 h of observations were included in the analysis. The differential spectrum of the 800 GeV–10 TeV emission is fitted well with a power law $dF/dE = (1.21 \pm 0.19) \times 10^{-12} (E/\text{TeV})^{-2.89 \pm 0.16} \text{ TeV}^{-1} \text{ cm}^{-2} \text{ s}^{-1}$, with $\chi^2/DoF = 0.74$ (where $DoF = 6$). The IC 443 gamma-ray emission characteristics are presented in Figure 4) with the spectral energy distribution and emission map viewed by SHALON in comparison with experiment data [24,30,53,60] and theoretical predictions (see Figure 4, [60]).

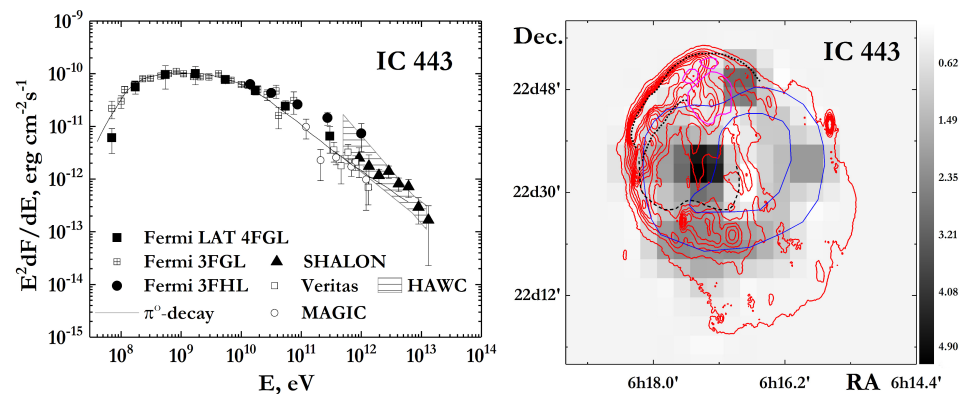


Figure 4. (left): Spectral energy distribution of IC 443 SNR: \blacktriangle at TeV energies show the data from SHALON observations. (right): Emission map of SNRs by SHALON (grey scale). Red lines show Canadian Galactic Plane Survey DRAO data; magenta lines are the X-ray data by XMM-Newton, and blue lines show MeV-GeV emission regions by Fermi LAT (see text for the description).

The IC 443 TeV structure by SHALON (Figure 4, grey scale) is overlaid with 1420 MHz CGPS DRAO contours [51] and high energy data from Fermi-LAT. The Veritas observations reveal the emission region which correlates with one from Fermi-LAT data [61]. It was found that 800 GeV–10 TeV γ -ray emission maxima correlate with MeV-GeV emission observed by Fermi-LAT [60] (Figure 4, blue contours). Also MeV-GeV and TeV γ -ray emission from the South and South-West parts of IC 443 shell coincides with the position of swept out dense molecular cloud (see black dotted and dashed lines and red contours by CGPS in Figure 4).

The hadronic scenario is considered as favored for the production of the 100 MeV–10 TeV gamma-emission from the IC 443. It is supposed that the γ -rays are generated in the IC443 SNR shell through the π^0 -decay which is produced in the interactions of the cosmic rays with the interstellar gas (Figure 4, solid line, [60]). The considered hadronic scenario supposes the 1–10% efficiency of cosmic ray acceleration [62]. It should be noted that no bright source of seed photons in the region of the IC 443 was found to support the leptonic mechanism of generation of detected gamma-rays. The location of 1.4–5.0 keV X-ray emission region by XMM-Newton [63] experiment is shown using the magenta lines in Figure 4. So, the Inverse Compton scattering cannot explain the observed high and very-high γ -ray emission from IC 443.

6. G166.0+4.3

Being of an unusual structure G166.0+4.3 (VRO 42.05.01) is referred to as a mixed-morphology supernova remnant that displays a shell-like morphology in the radio but in

the X-rays, they are centrally dominating. G166.0+4.3 distance is estimated as 5 kpc and an age of $\sim 2.4 \times 10^4$ years.

The G166.0+4.3 SNR looks very different at X-rays and radio energies. An outstanding edge-brightened shape of the shell and “wing” component is visible in radio wavelength [64]. Whereas thermal X-ray emission dominates by a bright spot within the “wing” component [65]; its image is not edge-brightened. It is supposed that the observed SNR morphology is a result of the expansion of the shock waves in the medium of different densities. The propagating through the high-dense medium shock viewed as a circular component meets the low-density medium forming the wing-shaped component. Due to this phenomenon of the shock encountering a density discontinuity in the interstellar medium, G166.0+4.3 became a candidate for the investigation of particle acceleration in SNR shocks at high- and very high energies.

The gamma-ray emission of 50 MeV–100 GeV from G166.0+4.3 corresponding to the radio structures has been detected with the Fermi-LAT 12-year observation data [24,66]. The spectrum of high energy emission is described by a power law with an index of -2.55 ± 0.06 [24]. G166.0+4.3 was observed with SHALON telescope during moonless nights with zenith angles from 5° to 35° in period of 2015–2016 years. The data analysis includes the 39.2 h of observations using the standard procedure of SHALON experiment [9,10,27]. The gamma-ray emission at energy above 800 GeV from G166.0+4.3 SNR was detected by SHALON with a statistical significance of 11.3σ [13]. The G166.0+4.3 integral flux above 0.8 TeV is $I_{G166.0+4.3}(> 0.8 \text{ TeV}) = (1.23 \pm 0.16) \times 10^{-12} \text{ cm}^{-2} \text{ s}^{-1}$ [15]. The differential spectrum of gamma-rays in the energy range of from 0.8 TeV to 10 TeV is obtained by SHALON and it is well fitted with a power law $dF/dE = (1.44 \pm 0.33) \times 10^{-12} (E/\text{TeV})^{-2.65 \pm 0.19}$, with $\chi^2/\text{DoF} = 1.79$ (where $\text{DoF} = 7$). The power-law with exponential cutoff fit to the data points of G166.0+4.3 spectrum: $dF/dE = (1.45 \pm 0.21) \times 10^{-12} (E/\text{TeV})^{-1.23 \pm 0.40} \times \exp(-E/(2.45 \pm 0.90)\text{TeV})$ gives χ^2 of 0.69 for six degrees. The spectral energy distribution of G166.0+4.3 at TeV energy range is shown in Figure 5 together with Fermi LAT [24] data at MeV-GeV energies. Figure 5 bottom presents 1420 MHz radio contours of G166.0+4.3 from Canadian Galactic Plane Survey DRACO [51] and X-ray 0.52–2.02 keV image by ROSAT (RASS 3 processing) [65] overlaid with TeV structure in energy range of 0.8–7 TeV by SHALON (grey-scale). Also, the 2–100 GeV emission by Fermi-LAT [66] is shown with blue lines in Figure 5.

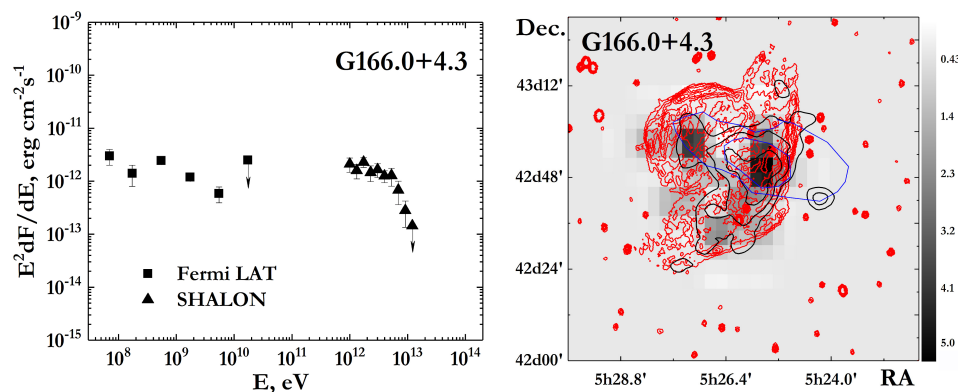


Figure 5. (left): Spectral energy distribution of G166.0+4.3 SNRs: \blacktriangle at TeV energies show the data from SHALON observations. (right): Emission map of SNR by SHALON (grey scale). Red lines show Canadian Galactic Plane Survey DRACO data; black contours are the X-ray data by ROSAT, and blue lines show MeV-GeV emission regions by Fermi LAT (see text for the description).

The structures viewed in TeV γ -rays correlate with the North-East and South-West parts of components visible in the radio energies by CGPS (red contours in Figure 5, bottom). However, GeV and TeV emission is more significant near the West, where the maximum of X-ray emission (black contours in Figure 5) viewed by ROSAT [65] are located. So, the position of GeV, TeV, and X-ray maxima corresponds to the extended wing component.

Both the leptonic and hadronic origins of observed gamma-ray emission in G166.0+4.3 are considered. As proposed in [66] the leptonic scenario for the high energy emission is compatible with the parameters of the environment and high energy particle population implied by X-ray observations. On the other hand, the HI observations [67] revealed that the G166.0+4.3 SNR is interacting with the interstellar medium, and considering the low ambient density revealed from ROSAT X-ray data [65] the hadronic interpretation of the detected gamma-ray emission is favored. However, there is not enough understanding of the G166.0+4.3 morphology, namely the conditions for the interactions of SNR shocks and the parameters of the surrounding medium, giving a rise the peculiar shape of this object.

7. Conclusions

The investigations of different-morphology Galactic supernova remnants staying on different evolution stages across the electromagnetic spectrum from radio up to very high energy gamma-rays were discussed. The characteristics of supernova remnants Cas A, Tycho's SNR, γ Cygni SNR, IC 443, and G166.0+4.3 in the wide energy range including the 800 GeV–100 TeV data from observations by the SHALON experiment were presented. The study aimed to identify the nature of the emission observed at high and very high energies and thus to reveal whether the cosmic rays are generated with these SNRs or not. The spectral energy distributions of discussed objects were presented together with estimations and theoretical models of gamma-ray production in SNRs. The SNRs' emission maps obtained through the different energy bands including radio, X-ray, MeV-GeV, and TeV gamma-rays then overlaid show essential features of morphology as a forward and reverse shock or the location of swept-out dense molecular clouds. The experimental data presented confirmed the scenario predicted within the discussed models with the hadronic origin of high and very high energy 800 GeV–100 TeV gamma-rays in Tycho's SNR, Cas A, and IC 443. The results of observations of γ Cygni SNR and G166.0+4.3 SNRs, also, point to the hadronic origin of the detected high and very high energy emissions, but still, investigations are needed to reveal the conditions for the interactions of SNR shocks and the parameters of the surrounding medium that give a rise to the peculiar morphology of these objects. The presented experimental data collected at the very high energy range favor a hadronic origin of observed gamma-ray emission within the considered estimations and models and further can help to make clear the contribution of SNRs on the different steps of evolution to the production of galactic cosmic rays.

Author Contributions: All authors contributed equally. All authors have read and agreed to the published version of the manuscript.

Funding: This research was funded by Russian Academy of Science in the framework of support of long-term studies.

Conflicts of Interest: The authors declare no conflict of interest.

References

1. Ginzburg, V.L.; Syrovatskii, S.I. *The Origin of Cosmic Rays*; Pergamon Press: Oxford, UK, 1964.
2. Berezhko, E.G.; Krymskii, G.F. Acceleration of cosmic rays by shock waves. *Usp. Fiz. Nauk* **1988**, *154*, 27–51. [[CrossRef](#)]
3. Reynolds, S.P. Supernova Remnants at High Energy. *Ann. Rev. Astronomy. Astrophysics*. **2008**, *46*, 89–126. [[CrossRef](#)]
4. Krymskii, G.F. A regular mechanism for the acceleration of charged particles on the front of a shock wave. *Akademiia Nauk SSSR Doklady* **1977**, *234*, 1306–1308.
5. Völk, H.J.; Berezhko, E.G.; Ksenofontov, L.T. Internal dynamics and particle acceleration in Tycho's SNR. *Astron. Astrophys.* **2008**, *483*, 529–535. [[CrossRef](#)]
6. Bell, A.R. The acceleration of cosmic rays in shock fronts – I. *Mon. Notices Royal Astron. Soc.* **1978**, *182*, 147–156. [[CrossRef](#)]
7. Nikolsky, S.I.; Sinitsyna, V.G. Investigation of gamma-sources by mirror telescope. In Proceedings of the International Workshop of Very High Energy Gamma-ray Astronomy, Crimea, USSR, 17–21 April 1989; p. 11.
8. Sinitsyna, V.G. Searches for gamma-quanta from local sources by a wide-angle imaging telescope. *Nuovo Cimento C* **1996**, *19*, 965–970. [[CrossRef](#)]
9. Sinitsyna, V.G.; Sinitsyna, V.Y. Emission from the galaxy NGC 1275 at high and very high energies and its origin. *Astron. Lett.* **2014**, *40*, 75–85. [[CrossRef](#)]

10. Sinitsyna, V.G.; Sinitsyna, V.Y.; Borisov, S.S.; Klimov, A.I.; Mirzafatikhov, R.M.; Moseiko, N.I. Very high energy astrophysics with the SHALON Cherenkov telescopes. *Nucl. Instrum. Methods Phys. Res. A* **2020**, *952*, 161775. [[CrossRef](#)]
11. Sinitsyna, V.G.; Arsov, T.P.; Alaverdyan, A.Y.; Borisov, S.S.; Galitskov, A.N.; Ivanov, I.A.; Kasparov, G.M.; Klevalin, V.A.; Malisko, A.A.; Musin, F.M.; et al. Stereoscopic Cherenkov Telescope System Shalon Alatoo. In Proceedings of the 27th International Cosmic Ray Conference (ICRC27), Hamburg, Germany, 7–15 August 2001; pp. 2798–2801.
12. Goncharkii, A.V.; Cherepashchuk, A.M.; Yagola, A.G. *Ill-Posed Problems in Astrophysics*; Nauka, Fizmatlit: Moscow, Russia, 1985.
13. Li, T.-P.; Ma, Y.-Q. Analysis methods for results in gamma-ray astronomy. *Astrophys. J.* **1983**, *272*, 317–324. [[CrossRef](#)]
14. Sinitsyna, V.G. SHALON. In Proceedings of the International Workshop, Towards a Major Atmospheric Cherenkov Detector V, Kruger Park, South Africa, 8–11 August 1997; De Jager, O., Ed.; Westprint: Potchefstroom, South Africa, 1997; pp. 190–195.
15. Sinitsyna, V.G.; Sinitsyna, V.Y.; Borisov, S.S.; Ivanov, I.A.; Klimov, A.I.; Mirzafatikhov, R.M.; Moseiko, N.I. Shell-type supernova remnants as sources of cosmic rays. *Adv. Space Res.* **2018**, *62*, 2845–285. [[CrossRef](#)]
16. Chevalier, R.A.; Oishi, J. Cassiopeia A and its clumpy presupernova wind. *Astrophys. J.* **2003**, *593*, L23. [[CrossRef](#)]
17. Bell, A.R.; Gull, S.F.; Kenderdine, S. New radio map of Cassiopeia A at 5 GHz. *Nature* **1975**, *257*, 463–465. [[CrossRef](#)]
18. Kassim, N.E.; Perley, R.A.; Dwarakanath, K.S.; Erickson, W.C. Evidence for thermal absorption inside Cassiopeia A. *Astrophys. J.* **1995**, *455*, L59. [[CrossRef](#)]
19. DeLaney, T.; Kassim, N.E.; Rudnick, L.; Perley, R.A. The density and mass of unshocked ejecta in Cassiopeia a through low frequency radio absorption. *Astrophys. J.* **2014**, *785*, 7. [[CrossRef](#)]
20. Hwang, U.; Laming, J.M.; Badenes, C.; Berendse, F.; Blondin, J.; Cioffi, D.; DeLaney, T.; Dewey, D.; Fesen, R.; Flanagan, K.A. A million second Chandra view of Cassiopeia A. *Astrophys. J.* **2004**, *615*, L117. [[CrossRef](#)]
21. Grefenstette, B.W.; Reynolds, S.P.; Harrison, F.A.; Humensky, T.B.; Boggs, S.E.; Fryer, C.L.; DeLaney, T.; Madsen, K.K.; Miyasaka, H.; Wik, D.R. Locating the most energetic electrons in Cassiopeia A. *Astrophys. J.* **2015**, *802*, 15. [[CrossRef](#)]
22. Wei Wang, W.; Li, Z. Hard X-ray emissions from Cassiopeia A observed by INTEGRAL. *Astrophys. J.* **2016**, *825*, 102. [[CrossRef](#)]
23. Abdo, A.A.; Ackermann, M.; Ajello, M.; Allafort, A.; Baldini, L.; Ballet, J.; Barbiellini, G.; Baring, M.G.; Bastieri, D.; Baughman, B.M. et al. Fermi-LAT discovery of GeV gamma-ray emission from the young supernova remnant Cassiopeia A. *Astrophys. J.* **2010**, *710*, L92. [[CrossRef](#)]
24. Abdollahi, S.; Acero, F.; Baldini, L.; Bastieri, D.; Bellazzini, R.; Berenji, B.; Berretta, A.; Bissaldi, E.; Blandford, R.D.; Zaharijas, G.; et al. Incremental Fermi Large Area Telescope Fourth Source Catalog *Astrophys. J., Suppl. Ser.* **2022**, *260*, 53. [[CrossRef](#)]
25. Acciari, V.A.; Aliu, E.; Arlen, T.J.; Aune, T.; Bautista, M.; Beilicke, M.; Benbow, W.; Boltuch, D.; Bradbury, S. M.; Buckley, J. H. et al. Observations of the shell-type supernova remnant Cassiopeia A at TeV energies with VERITAS. *Astrophys. J.* **2010**, *714*, 163. [[CrossRef](#)]
26. Berezhko, E.G.; Pühlhofer, G.; Völk, H.J.; Ksenofontov, L.T. Gamma-ray emission from Cassiopeia A produced by accelerated cosmic rays. *Astron. Astrophys.* **2003**, *400*, 971–980. [[CrossRef](#)]
27. Sinitsyna, V.G.; Sinitsyna, V.Y. Supernova remnants: The Crab Nebula, Cassiopeia A, and Tycho as sources of cosmic rays in our galaxy. *Astron. Lett.* **2011**, *37*, 621–634. [[CrossRef](#)]
28. Sinitsyna, V.G.; Sinitsyna, V.Y. Generation of Cosmic rays in Shell-type and PWN Supernova Remnants. *Astroparticle, Particle, Space Physics and Detectors Physics Applications*; Giani, S., Leroy, C., Rancoita, P.-G., Price, L., Ruchti, R., Eds.; World Scientific: Singapore, 2014; Volume 8, p. 135.
29. Zirakashvili, V.N.; Aharonian, F.; Yang, R.; Oña-Wilhelmi, E.; Tufts, R.J.; et al. Nonthermal radiation of young supernova remnants: The case of Cas A. *Astrophys. J.* **2014**, *785*, 130. [[CrossRef](#)]
30. Ajello, M.; Atwood, W.B.; Baldini, L.; Ballet, J.; Barbiellini, G.; Bastieri, D.; Bellazzini, R.; Bissaldi, E.; Blandford, R.D.; Bloom, E.D. et al. The third catalog of hard Fermi-LAT sources. *Astrophys. J., Suppl. Ser.* **2017**, *232*, 18. [[CrossRef](#)]
31. Abeyssekara, A.U.; Archer, A.; Benbow, W.; Bird, R.; Brose, R.; Buchovecky, M.; Buckley, J.H.; Chromey, A.J.; Cui, W.; Daniel, M.K. et al. Evidence for Proton Acceleration up to TeV Energies Based on VERITAS and Fermi-LAT Observations of the Cas A SNR. *Astrophys. J.* **2020**, *894*, 51. [[CrossRef](#)]
32. Ahnen, M.L.; Ansoldi, S.; Antonelli, L.A.; Arcaro, C.; Babić, A.; Banerjee, B.; Bangale, P.; Barres de Almeida, U.; Barrio, J. A.; Becerra González, J. et al. A cut-off in the TeV gamma-ray spectrum of the SNR Cassiopeia A. *Mon. Notices Royal Astron. Soc.* **2017**, *472*, 2956. [[CrossRef](#)]
33. Fleischhack, H. A Survey of TeV Emission from Galactic Supernova Remnants with HAWC. In Proceedings of the 36th ICRC, Madison, WI, USA, 24 July–1 August 2019; Volume 36, p. 674.
34. Gotthelf, E. V.; Koralesky, B.; Rudnick, L.; Jones, T.W.; Hwang, U.; Petre, R. Chandra detection of the forward and reverse shocks in Cassiopeia A. *Astrophys. J.* **2001**, *552*, L39. [[CrossRef](#)]
35. Krause, O.; Tanaka, M.; Usuda, T.; Hattori, T.; Goto, M.; Birkmann, S.; Nomoto, K.I. Tycho Brahe’s 1572 supernova as a standard type Ia as revealed by its light-echo spectrum. *Nature* **2008**, *456*, 617–619. [[CrossRef](#)]
36. Hayato, A.; Yamaguchi, H.; Tamagawa, T.; Katsuda, S.; Hwang, U.; Hughes, J.P.; Ozawa, M.; Bamba, A.; Kinugasa, K.; Terada, Y. et al. Expansion velocity of ejecta in Tycho’s supernova remnant measured by doppler broadened x-ray line emission. *Astrophys. J.* **2010**, *725*, 894.

- [CrossRef]
37. Warren, J.S.; Hughes, J.P.; Badenes, C.; Ghavamian, P.; McKee, C.F.; Moffett, D.; Plucinsky, P.P.; Rakowski, C.; Reynoso, E.; Slane, P. Cosmic-Ray Acceleration at the Forward Shock in Tycho's Supernova Remnant: Evidence from Chandra X-Ray Observations. *Astrophys. J.* **2005**, *634*, 376. [CrossRef]
 38. Sinitsyna, V.G. Galactic and Extragalactic sources of Very High Energy of Gamma-Quanta. In Proceedings of the Workshop on TeV Astro/Particle Physics, Towards a Major Atmospheric Cherenkov Detector-V, Kruger Park, South Africa, 8–11 August 1997; De Jager, O., Ed.; Westprint: Potchefstroom, South Africa, 1997; p. 136.
 39. Sinitsyna, V.G.; Alaverdyan, A.Y.; Ivanov, I.A.; Nikolsky, S.I.; Musin, F.M.; Mirzafatihov, R.M.; Platonov, G.F.; Sinitsyna, V.Y.; Oblakov, I.V. TeV gamma-ray emission from point sources: galactic and extragalactic. *Nucl. Phys. B (Proc. Suppl.)* **2001**, *97*, 215–218. [CrossRef]
 40. Acciari, V.A.; Aliu, E.; Arlen, T.; Aune, T.; Beilicke, M.; Benbow, W.; Bradbury, S.M.; Buckley, J.H.; Bugaev, V.; Byrum, K. et al. Discovery of TeV gamma-ray emission from Tycho's supernova remnant. *Astrophys. J.* **2011**, *730*, L20. [CrossRef]
 41. Kosenko, D.; Blinnikov, S.I.; Vink, J. Modeling supernova remnants: effects of diffusive cosmic-ray acceleration on the evolution and application to observations. *Astron. Astrophys.* **2011**, *532*, A114. [CrossRef]
 42. Lozinskaya, T.A.; Pravdikova, V.V.; Finoguenov, A.V. The supernova remnant G78. 2+ 2.1: New optical and X-ray observations. *Astron. Lett.* **2000**, *26*, 77–87. [CrossRef]
 43. Truemper, J. The ROSAT mission. *Adv. Space Res.* **1983**, *2*, 241–249. [CrossRef]
 44. Leahy, D.A.; Green, K.; Ranasinghe, S. X-ray and radio observations of the γ Cygni supernova remnant G78.2+ 2.1. *Mon. Notices Royal Astron. Soc.* **2013**, *436*, 968–977. [CrossRef]
 45. Tanaka, Y.; Inoue, H.; Holt, S.S. The X-ray astronomy satellite ASCA. *Publ. Astron. Soc. Jpn.* **1994**, *46*, L37–L41.
 46. Uchiyama, Y.; Takahashi, T.; Aharonian, F.A.; Mattox, J.R. ASCA View of the Supernova Remnant γ Cygni (G78.2+ 2.1): Bremsstrahlung X-Ray Spectrum from Loss-flattened Electron Distribution. *Astrophys. J.* **2002**, *571*, 866. [CrossRef]
 47. Hartman, R.C.; Bertsch, D.L.; Bloom, S.D.; Chen, A.W.; Deines-Jones, P.; Esposito, J.A.; Fichtel, C.E.; Friedlander, D.P.; Hunter, S.D.; McDonald, L.M. et al. The third EGRET catalog of high-energy gamma-ray sources. *Astrophys. J., Suppl. Ser.* **1999**, *123*, 79. [CrossRef]
 48. Castro, D.; Slane, P.; Patnaude, D.J.; Ellison, D.C. The Impact of Efficient Particle Acceleration on The Evolution of Supernova Remnants in the Sedov–Taylor Phase. *Astrophys. J.* **2011**, *734*, 85. [CrossRef]
 49. Ackermann, M.; Ajello, M.; Baldini, L.; Ballet, J.; Barbiellini, G.; Bastieri, D.; Bellazzini, R.; Bissaldi, E.; Bloom, E. D.; Bonino, R.; et al. Search for extended sources in the galactic plane using six years of Fermi-Large Area Telescope pass 8 data above 10 GeV. *Astrophys. J.* **2017**, *843*, 139. [CrossRef]
 50. Sinitsyna, V.G.; Sinitsyna, V.Y. Long-term observations of the Cyg X-3 and γ Cygni SNR at ultrahigh energies by SHALON mirror Cherenkov telescopes. *Bulletin of the Lebedev Physics Institute* **2013**, *40*, 113–118. [CrossRef]
 51. Taylor, A.R.; Gibson, S.J.; Peracaula, M.; Martin, P. G.; Landecker, T. L.; Brunt, C. M.; Dewdney, P. E.; Dougherty, S. M.; Gray, A. D.; Higgs, L. A. et al. The Canadian galactic plane survey. *Astrophys. J.* **2003**, *125*, 3145.
 52. Weinstein, A. Detection of VER J2019+407 (G78.2+2.1) and Tycho's Supernova Remnant with VERITAS. In Proceedings of the 2011 Fermi Symposium, Rome, Italy, 9–11 May 2011 *eConf Proceedings*, C110509.
 53. Albert, A.; Alfaro, R.; Alvarez, C.; Angeles Camacho, J.R.; Arteaga-Velázquez, J.C.; Arunbabu, K.P.; Avila Rojas, D.; Ayala Solares, H.A.; Baghmany, V.; Belmont-Moreno, E. et al. 3HWC: The third HAWC catalog of very-high-energy gamma-ray sources. *Astrophys. J.* **2020**, *905*, 76. [CrossRef]
 54. Abeyskara, A.U.; Albert, A.; Alfaro, R.; Alvarez, C.; Álvarez, J. D.; Arceo, R.; Arteaga-Velázquez, J.C.; Ayala Solares, H.A.; Barber, A.S.; Baughman, B. et al. The 2HWC HAWC observatory gamma-ray catalog. *Astrophys. J.* **2017**, *843*, 40. [CrossRef]
 55. Aliu, E.; Archambault, S.; Arlen, T.; Aune, T.; Beilicke, M.; Benbow, W.; Bird, R.; Bouvier, A.; Bradbury, S.M.; Buckley, J.H. et al. Discovery of TeV gamma-ray emission toward supernova remnant SNR G78.2+ 2.1. *Astrophys. J.* **2013**, *770*, 93. [CrossRef]
 56. Gosachinskij, I.V. HI Distribution in the Region of the Supernova Remnant G78.2+ 2.1. *Astron. Lett.* **2001**, *27*, 233–238. [CrossRef]
 57. Lee, J.-J.; Koo, B.-C.; Snell, R.L.; Yun, M.S.; Heyer, M.H.; Burton, M.G. Identification of ambient molecular clouds associated with galactic supernova remnant IC 443. *Astrophys. J.* **2012**, *749*, 34. [CrossRef]
 58. Lee, J.-J.; Koo, B.-C.; Yun, M.S.; Stanimirović, S.; Heiles, C.; Heyer, M. A 21 cm spectral and continuum study of IC 443 using the very large array and the Arecibo telescope. *Astron. J.* **2008**, *135*, 796. [CrossRef]
 59. Sinitsyna, V.G.; Sinitsyna, V.Y. Cosmic ray production in historical supernova remnants. *J. Phys. Conf. Ser.* **2013**, *409*, 012110. [CrossRef]
 60. Abdo, A.A.; Ackermann, M.; Ajello, M.; Baldini, L.; Ballet, J.; Barbiellini, G.; Bastieri, D.; Baughman, B. M.; Bechtol, K.; Bellazzini, R.; et al. Observation of supernova remnant IC 443 with the Fermi large area telescope. *Astrophys. J.* **2010**, *712*, 459. [CrossRef]
 61. Humensky, B. The TeV Morphology of the Interacting Supernova Remnant IC 443. In Proceedings of the 34th ICRC, The Hague, The Netherlands, 30 July–6 August 2015; PoS(ICRC2015)875.
 62. Tavani, M.; Giuliani, A.; Chen, A.W.; Argan, A.; Barbiellini, G.; Bulgarelli, A.; Caraveo, P.; Cattaneo, P.W.; Cocco, V.; Contessi, T. et al. Direct evidence for hadronic cosmic-ray acceleration in the supernova remnant IC 443. *Astrophys. J. Lett.* **2010**, *710*, L151. [CrossRef]
 63. Troja, E.; Bocchino, F.; Miceli, M.; Reale, F. XMM-Newton observations of the supernova remnant IC 443-II. Evidence of stellar ejecta in the inner regions. *Astron. Astrophys.* **2008** *485*, 777–785. [CrossRef]

64. Pineault, S.; Pritchett, C.; Landecker, T.L.; Routledge, D.; Vaneldik, J.F. Optical and radio imaging of the supernova remnant VRO 42.05.01 (G166.0+4.3). *Astron. Astrophys.* **1985**, *151*, 52–60.
65. Burrows, D.N.; Guo, Z. ROSAT observations of VRO 42.05.01. *Astrophys. J.* **1994**, *421*, L19–L22. [[CrossRef](#)]
66. Araya, M. Detection of gamma-ray emission in the region of the supernova remnants G296.5+10.0 and G166.0+4.3. *Mon. Notices Royal Astron. Soc.* **2013**, *434*, 2202–2208. [[CrossRef](#)]
67. Landecker, T.L.; Pineault, S.; Routledge, D.; Vaneldik, J.F. The interaction of the supernova remnant VRO 42.05.01 with its H I environment. *Mon. Notices Royal Astron. Soc.* **1989**, *237*, 277–297. [[CrossRef](#)]

Disclaimer/Publisher’s Note: The statements, opinions and data contained in all publications are solely those of the individual author(s) and contributor(s) and not of MDPI and/or the editor(s). MDPI and/or the editor(s) disclaim responsibility for any injury to people or property resulting from any ideas, methods, instructions or products referred to in the content.